Systematics of fission barriers in superheavy elements

T. Bürvenich,[1] M. Bender,[2] J. A. Maruhn,[3,4] and P.-G. Reinhard[4,5]
[1]*Theoretical Division, Los Alamos National Laboratory, Los Alamos, New Mexico 87545, USA*
[2]*Service de Physique Nucléaire Théorique, Université Libre de Bruxelles, CP 229, B-1050 Brussels, Belgium*
[3]*Institut für Theoretische Physik, Universität Frankfurt, Robert-Mayer-Strasse 8-10, D-60325 Frankfurt am Main, Germany*
[4]*Joint Institute for Heavy-Ion Research, Oak Ridge National Laboratory, P. O. Box 2008, Oak Ridge, Tennessee 37831, USA*
[5]*Institut für Theoretische Physik II, Universität Erlangen-Nürnberg, Staudtstrasse 7, D-91058 Erlangen, Germany*
(Received 14 February 2003; published 23 January 2004; corrected 30 January 2004)

We investigate the systematics of fission barriers in superheavy elements in the range $Z=108-120$ and $N=166-182$. Results from two self-consistent models for nuclear structure, the relativistic mean-field (RMF) model as well as the nonrelativistic Skyrme-Hartree-Fock approach are compared and discussed. We restrict ourselves to axially symmetric shapes, which provides an upper bound on static fission barriers. We benchmark the predictive power of the models examining the barriers and fission isomers of selected heavy actinide nuclei for which data are available. For both actinides and superheavy nuclei, the RMF model systematically predicts lower barriers than most Skyrme interactions. In particular, the fission isomers are predicted too low by the RMF, which casts some doubt on recent predictions about superdeformed ground states of some superheavy nuclei. For the superheavy nuclei under investigation, fission barriers drop to small values around $Z=110$, $N=180$, and increase again for heavier systems. For most of the forces, there is no fission isomer for superheavy nuclei, as superdeformed states are in most cases found to be unstable with respect to octupole distortions.

DOI: 10.1103/PhysRevC.69.014307 PACS number(s): 21.30.Fe, 21.60.Jz, 24.10.Jv, 27.90.+b

I. INTRODUCTION

The search for superheavy elements (SHE) has made exciting progress in the past few years [1–3]. New, often more neutron-rich, isotopes of elements $Z=108$ [4], $Z=110$ [5], and $Z=112$ [6] have been reported as well as the synthesis of the new elements $Z=114$ [7] and $Z=116$ [8]. At the same time earlier experiments were confirmed and more data for already existing isotopes collected [9]. Together with the α-decay products of the newly synthesized nuclei the known region of superheavy elements has grown substantially.

SHE are by definition those nuclei at the upper end of the chart of nuclei where quantum-mechanical shell effects reverse the trend of decreasing—and, for the heavier ones, practically vanishing—liquid-drop fission barriers to produce significant stabilization. The lifetimes of the recently found SHE are many orders of magnitude smaller than the early optimistic estimates [10,11]. Additionally, the systematics of fusion cross sections suggests that the extension of the chart of nuclides might be limited by the production mechanism of SHE, not their decay [3]. With recent experiments heading for unknown territory, theory has to provide reliable predictions for the stability and the most accessible regions in the landscape of nuclides. A crucial feature is here spontaneous fission which is characterized by the fission barrier.

Not too much is known experimentally on the fission barriers of transfermium nuclei. Although their height is not known, barriers for ^{252}No and ^{254}No are high enough to stabilize these isotopes against fission up to angular momentum 20 [12]. An analysis of all available data for fusion and fission of ^{292}112, ^{292}114, and ^{296}116 was given recently in Ref. [13]. Surprisingly, the barrier heights deduced for these very heavy nuclei are similar, or even slightly larger, than the ones of actinide nuclei in the ^{240}Pu region.

For some other superheavy nuclei it is known that the barrier is relatively small from the simple fact that fission is their preferred decay channel. This leads to another aspect of the stability against fission: the experimental identification of new superheavy nuclides is much simpler when α decay is the dominating decay channel. All recent new decay chains from Dubna end in a region of fissioning nuclei which prevents an extension of the known region of SHE to the "southeast" with current experimental techniques.

The calculation of fission half-lives is a very demanding task, which became clear quite early [14]. First explorations of the potential energy surfaces of transfermium nuclei demonstrated already that triaxial and reflection-asymmetric degrees of freedom often greatly reduce the fission barrier. The collective mass provides the metric for the dynamical calculation of the fission half-lives. There is no published work so far that considers all ingredients using self-consistent models. First ambitious steps in that direction were taken for the calculation of the decay of the fission isomer into the ground state [15]. The published fission half-lives from macroscopic-microscopic mean-field models also simplify the task considerably by restricting shape degrees of freedom to axially symmetric ones and using a phenomenological parametrization of inertia parameters. The detailed potential energy landscape is also an ingredient for estimates on the fusion cross section, although somewhat different paths have to be considered asymptotically, see e.g. Ref. [16] and further references therein.

It is the aim of this paper to analyze the extrapolation of self-consistent mean-field models, namely, the Skyrme-Hartree-Fock (SHF) approach and the relativistic mean-field (RMF) model, concerning large-amplitude deformation properties of SHE. To that end, we present a systematic survey of fission paths and barriers for a broad range of SHE, scanning the α-decay chains of even-even nuclei that are accessible with the current experimental techniques. The nuclei consid-

 ©2004 The American Physical Society

ered in this study cover the proton numbers $108 \leqslant Z \leqslant 120$ and the corresponding neutron numbers $166 \leqslant N \leqslant 182$. We first benchmark our models by calculating axial fission barriers and isomeric states for heavy actinide nuclei for which experimental data are available, namely, isotopes with proton numbers ranging from $Z=90$ to 98.

Section II summarizes the most important results of earlier studies relevant for our calculations. Section III explains the theoretical and numerical methods which are used in our study. In Sec. IV the results for actinides are discussed. Section V presents detailed results for deformation energy curves in all considered superheavy nuclei and for all the different forces. Section VI discusses the result in terms of key quantities such as deformation energies and barriers. Finally, Sec. VII attempts to identify the underlying reasons for the different predictions among the forces and models.

II. EARLIER CALCULATIONS

Estimates of the stability of SHE against fission have a long history. First explorations of the potential landscapes were made with phenomenological corrections for shell effects [11,17], even before Strutinsky introduced the microscopic-macroscopic method [18], which was then immediately applied to large-scale calculations of fission barriers of heavy and superheavy nuclei, see e.g. Ref. [19]. In this framework, the deformation energy is minimized in a limited space of shape parameters. It soon became clear that reflection-asymmetric [20] and triaxial [21] shape degrees of freedom have to be included. Complementing the collective potential energy surfaces by mass parameters enabled the calculation of fission half-lives of heavy and superheavy nuclei, with phenomenological mass parameters [10,22] as well as with microscopically computed cranking masses [23]. Studies along that line are continued till today with improved parametrizations of the microscopic-macroscopic (mic-mac) model, either the finite-range droplet model plus folded-Yukawa single-particle potential model and phenomenological masses [24] or the Yukawa-plus-exponential (YPE) macroscopic plus a Woods-Saxon microscopic model and cranking masses [25–27]. Nearly all large-scale calculations of fission lifetimes, however, consider axially symmetric shapes only (as we will do). A recent exception is presented in Ref. [27] where triaxial shapes are taken into account, however, at the price of a reduced number of shape degrees of freedom in other places.

There do exist also systematic calculations of fission barriers where the macroscopic part of the energy is calculated within the semi-classical Thomas-Fermi approximation [28]. One step further toward self-consistency is the extended Thomas-Fermi Strutinsky-integral (ETFSI) approach where the same microscopic Skyrme force is used to calculate the macroscopic part of the binding energy and to determine the single-particle spectra for the calculation of the shell correction. For a large-scale survey of the axially and reflection-symmetric potential energy surfaces of heavy and superheavy nuclei in the ETFSI approach using the Skyrme interaction SkSC4, see Refs. [29,30]. Results allowing also for triaxial degrees of freedom are presented for selected nuclei in Ref. [31].

To determine the fission path in microscopic-macroscopic, Thomas-Fermi, and ETFSI calculations, the total energy is minimized with respect to parameters of the nuclear shape. There are numerous parametrizations to be found in the literature, which differ by emphasizing either high-order multipoles at small deformation, or the fragment deformation of two-center-type configurations at large deformations, see Ref. [32] for an overview. While the latter are important for the proper description of the saddle point of actinide nuclei (which is located at very large β_2), the first might be better suited for superheavy nuclei where the saddle point is located at rather small β_2. The number of shape degrees of freedom in actual calculations does rarely exceed five, in most cases it is even smaller.

This restriction does not exist in the framework of self-consistent models. Besides very general spatial symmetries that are imposed (e.g., axiality, reflection symmetry, or triaxiality) there are no further assumptions made on the nuclear density distribution. As this makes self-consistent calculations more costly in terms of computational time, there is much less published work employing self-consistent models so far.

A systematic study of the deformation energy of superheavy nuclei along the valley of β stability in the region $100 \leqslant Z \leqslant 128$ and $150 \leqslant N \leqslant 218$ in HFB calculations with the Gogny force D1s under restriction to axially and reflection-symmetric shapes was presented in Ref. [33]. Potential energy surfaces of selected heavier nuclei are presented in Ref. [34]. The full potential energy surface in the β-γ plane of a few selected nuclei as resulting from SHF calculations in a triaxial representation is presented in Ref. [35]. This investigation points out the importance of triaxial shapes at small deformations $\beta_2 < 0.6$. The fission barrier of some superheavy nuclei is reduced to half its value when relaxing the constraint on axial symmetry and going through triaxial paths. The fission path returns to axially symmetric shapes at larger deformations. But here it is necessary to allow for reflection-asymmetric shapes to accommodate the usually asymmetric fission. A first exploration of asymmetric shapes of SHE within self-consistent SHF and RMF models was presented in Ref. [36]. For many superheavy systems, reflection-asymmetric shapes lower the fission path at large prolate deformation $\beta_2 > 0.6$, and remove in most cases the outer barrier known from actinide nuclei (and persisting for superheavy nuclei when considering reflection-symmetric shapes only).

III. THEORETICAL FRAMEWORK

A. Effective interactions

We explore the potential landscapes using two widely used self-consistent mean-field models, namely, the nonrelativistic SHF method as well as the RMF approach [37]. There exists a great variety of parametrizations for both models which often differ when extrapolated. It is long known that different parametrizations of a self-consistent model are not equivalent for the calculation of fission barriers of actinide nuclei, see Refs. [38,39] for a comparison of early Skyrme forces and Ref. [40] for a comparison of RMF

TABLE I. Compilation of bulk properties for the parametrizations employed in this study. The upper block shows the volume parameter incompressibility modulus K, effective mass m_0^*/m, and asymmetry energy coefficient $a_{\rm sym}$. The lower block shows the surface energy coefficient $a_{\rm surf}$ obtained from semi-infinite nuclear matter calculations. For the RMF, where the effective mass is momentum dependent, m_0^*/m is given at the Fermi momentum $k=k_{\rm F}$. This value, which is about 10% larger than the often quoted value for $k=0$, determines the average level density around the Fermi energy, see also Ref. [43] and references therein.

Force	SkP	SkI3	SkI4	SLy6	NL-Z2	NL3
K(MeV)	202	258	248	230	172	270
m_0^*/m	1.00	0.59	0.65	0.69	0.64	0.67
$a_{\rm sym}$(MeV)	30.0	34.8	29.5	32.0	39.0	37.4
$a_{\rm surf}$(MeV)	18.2	18.3	18.3	17.7	17.7	18.5

forces. Comparisons between SHF and RMF hint at genuine model differences [40,41]. Relevant for our study is also that there exist conflicting predictions for the location of the spherical magic numbers in SHE, see Refs. [42,43], which can be expected to be reflected in the structure of the potential landscapes.

A fair survey of the extrapolation of the models to large mass number and large deformation has therefore to cover a selection of typical parametrizations. We have chosen parametrizations which give a very satisfactory description of stable nuclei but differ in details. Namely, we use the Skyrme interactions SkP [44], SLy6 [45], SkI3, and SkI4 [46]. In the relativistic calculations the parametrizations NL3 [47] and NL-Z2 [43] of the standard Lagrangian are employed.

The parametrization SkP has the isoscalar effective mass $m_0^*/m=1$ and was originally designed to describe the particle-hole and particle-particle channel of the effective interaction simultaneously (we do not make use of this particular feature). The forces SLy6, SkI3, and SkI4 stem from recent fits including already data on exotic nuclei (all three forces) and even neutron matter (SLy6). Both SkP and SLy6 use the standard spin-orbit interaction. The forces SkI3/4 employ a spin-orbit force with modified isovector dependence. SkI3 contains a fixed isovector part analogous to the nonrelativistic limit of the RMF, whereas SkI4 is adjusted allowing free variation of the isovector spin-orbit term. The RMF force NL-Z2 is fitted in the same way as SkI3 and SkI4 to a similar set of observables.

A quantity that characterizes the average deformation properties of an effective interaction is the surface energy coefficient. It is determined for the model system of semi-infinite nuclear matter, which offers the cleanest procedure to define a surface energy, see, e.g., [37,48,49] and the references given therein. In Table I, we give values for bulk and surface properties of nuclear matter obtained exclusively in fully self-consistent Hartree-Fock calculations of semi-infinite matter [50,51]. Often values obtained within the extended Thomas-Fermi approximation are given [39], which are usually smaller by about 1 MeV.

A correction of the binding energy for spurious center-of-mass (c.m.) motion is performed as usual. For SkI3, SkI4, SLy6, and NL-Z2 the c.m. correction $E_{\rm c.m.}=\langle\hat{\mathbf{P}}_{\rm c.m.}^2\rangle/2mA$ is subtracted after variation. For SkP the diagonal part of $E_{\rm c.m.}$ only is considered before variation, while for NL3 the harmonic-oscillator estimate for $E_{\rm c.m.}$ is subtracted, see Ref. [41] for details. The c.m. correction, however, varies only little with deformation, see e.g. Refs. [41,52]. Note that the various recipes for c.m. correction cannot be easily interchanged as their differences are partially absorbed into the force parameters. This has a consequence relevant for our study. The difference between the "exact" and the approximate schemes used for SkP and NL3 scales in leading order as $\sim A^{2/3}$. During the fit this difference is incorporated into the effective interaction, which leads to the significantly larger surface tension for SkP and NL3 found in Table I, see Ref. [41]. The deformation energy from otherwise equally fitted forces might differ on the order of 5 MeV at the outer barrier in actinides. For SHE, where the saddle point is at smaller deformation, this effect can be expected to be less pronounced, but still might cause differences of a few MeV between forces.

We treat pairing correlations within the BCS approximation using an effective density-independent zero-range δ pairing force with the strength adjusted for each mean-field parametrization separately as described in Ref. [53]. Including a density dependence of the effective pairing interaction or an approximate particle-number projection might alter the barrier heights on the order of 1 MeV for actinide nuclei [54].

The coupled mean-field equations for both SHF and RMF models are represented on a grid in coordinate space using a Fourier representation of the derivatives and are solved with the damped gradient iteration method as described in Ref. [55]. The numerical codes for both models [54,56] share the same basic numerical routines which allows for a direct comparison of the results. Note that the accuracy of grid techniques is fairly independent of deformation, which is an advantage to calculations using a harmonic oscillator basis expansion; see, e.g., Ref. [52] for a convergence study for ^{256}Fm.

Finally, beyond-mean-field effects can modify the fission barrier. The most important corrections to the binding energy remove the contributions from spurious collective vibrational and rotational states which are inevitably admixed to the mean-field wave functions [37,52,57]. These corrections lower the barriers, typically up to 1 MeV for the inner one and up to 2 MeV for the outer when starting from a well-deformed prolate ground state. The situation is less clear for transitional or spherical nuclei.

Altogether, the present study has uncertainties on the deformation energy for given configuration of the order of 1–2 MeV. Most of the possible improvements increase the binding energy. Thus we can assume to explore an upper limit for the barriers. The comparison of barriers between different forces is more robust because most corrections can be expected to be similar for all forces.

B. Shape degrees of freedom

We will consider reflection-symmetric as well as reflection-asymmetric fission paths. But we restrict the con-

siderations to axially symmetric shapes. Our investigation also covers the prolate fission path only. It has to be kept in mind that novel fission paths may emerge for the heaviest of the nuclides discussed here, which start out from strongly oblate shapes and proceed through triaxial deformations [21]. For this and the reasons given above, our results provide an upper limit for the (static) fission barriers. This limitation holds also for most other work using self-consistent models published so far, as well as most of the results from mic-mac approaches.

The deformation energy curves are obtained with a constraint on the mass quadrupole moment $Q_{20}=\langle\hat{Q}_{20}\rangle$. For reflection-asymmetric shapes, we also fix the center of mass with a constraint on the mass dipole moment $\langle\hat{Q}_{10}\rangle=0$. The constraints are added to the energy functional by means of Lagrange multipliers [37]. Besides these constraints, the deformation energy is minimized with respect to all axial multipole moments $Q_{\ell 0}$ for protons and neutrons separately. In a self-consistent calculation, the energy is not only minimized with respect to the deformation, but also the radial profile of the density distribution, again separately for protons and neutrons. With that, a self-consistent calculation explores many more degrees of freedom than the best microscopic-macroscopic calculation available so far. Some consequences will be discussed in Sec. VI C below.

The deformation energy is shown versus the dimensionless multipole deformations of the mass density which are defined as

$$\beta_\ell = \frac{4\pi}{3Ar_0^\ell}\langle r^\ell Y_{\ell 0}\rangle \quad \text{with} \quad r_0 = 1.2A^{1/3}\ \text{fm}. \tag{1}$$

Note that the β_ℓ are computed from the expectation values of the actual shapes and need to be distinguished from the generating moments which are used in multipole expansions of the nuclear shape in microscopic-macroscopic models [32].

The constrained calculation does not always follow exactly the static fission path, which is defined as the path that follows the steepest descent in the multidimensional energy surface. Instead, for each value of Q_{20}, one obtains a state which corresponds to a minimum with respect to all other degrees of freedom [58]. This might cause some problems to keep track of the path whenever the fission path has a small component only in the direction of the constraint. Often there exist two or even more distinct valleys in the multidimensional potential landscape, which are separated by potential barriers. Depending on the choice for the initial wave functions, the constrained calculation might find the nearest relative minimum only, which is not necessarily the absolute minimum for a given constraint. The existence of distinct valleys complicates the interpretation of the deformation energy curves. When the solution jumps from one valley to another it misses the saddle point in between. The resulting uncertainty is not clear *a priori*, as only a calculation including two or even more constraints can clarify if there is a flat plateau or a mountain ridge between the two valleys. The change from one to another valley in the potential landscape is accompanied by discontinuities in higher multipole deformations which can be used to identify them. In some cases the existence of two distinct valleys might be the artifact of imposed symmetries, cf. the case of ^{258}Fm, where the two distinct valleys obtained from axially symmetric calculations are spurious as the two solutions are smoothly connected through triaxial shapes [36].

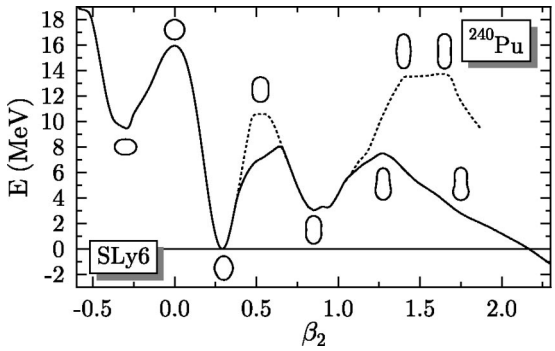

FIG. 1. Example for the double-humped fission barrier of the typical actinide nucleus ^{240}Pu. The dotted line denotes an axial and reflection-symmetric calculation, the full line denotes a triaxial (inner barrier) and axial and reflection-asymmetric calculation (outer barrier). The various shapes along the axial paths are indicated by the contours of the total density at $\rho_0=0.07$ fm^{-3}.

IV. BARRIERS IN ACTINIDE NUCLEI

Actinides are the heaviest nuclear systems for which data on the structure of the fission barrier are available. We use these nuclei to benchmark our models and forces, and to examine the force dependence of the predictions. We confine our investigation to axial barriers but release reflection symmetry in the calculations of the outer barriers and isomeric states.

There exists a wealth of information about the (in most cases) double-humped fission barriers of actinide nuclei, see Ref. [59] and references given therein. The generic features of the static fission path are shown in Fig. 1 for the example of ^{240}Pu calculated with the Skyrme force SLy6. The deformed ground state has a calculated deformation of $\beta_2=0.29$, which is in perfect agreement with the value of $\beta_2=0.29$ that can be deduced within the rigid rotor model from the $B(E2)\uparrow$ value of $13.33\pm0.18\ e^2\ \text{b}^2$ obtained from Coulomb excitation [60]. The deformation energy of 15.9 MeV of the ground state corresponds to 0.9% of the total binding energy. The inner barrier explores triaxial degrees of freedom, which reduce the (axial) barrier by about 3 MeV. There is a superdeformed fission isomer at $\beta_2\approx0.8$ at an excitation energy of 3.0 MeV, which is somewhat larger than the experimental value of 2.25 ± 0.20 MeV [61]. The outer barrier explores reflection-asymmetric shapes. The potential landscapes of adjacent actinide nuclei are similar, though for some nuclides there might appear a second isomeric state [62].

The double-humped fission barrier of ^{240}Pu has often served as a benchmark for mean-field models, see Ref. [63] for results obtained using Skyrme interactions, Ref. [64] using Gogny forces, Refs. [40,65] for the RMF, and Ref. [41]. Early comparisons of barriers obtained with different

Skyrme forces using approximations to full self-consistency were published in Refs. [38,39,66]. A direct comparison of the potential energy curves with triaxial inner and reflection-asymmetric outer barriers obtained with the Skyrme interactions SLy6, SkM*, and SkI4, the Gogny force D1s, and the RMF forces NL3 and NL-Z2 is presented in Ref. [37]. The excitation energy of the fission isomer has been studied with a variety of Skyrme forces in Refs. [67,68].

The influence of correlations on the deformation energy in the framework of Skyrme mean-field calculations has been studied in Ref. [69]. An exact angular momentum projection lowers the axial inner barrier by a bit less than 1 MeV, the excitation energy of the isomeric minimum by about 1 MeV, and the reflection-symmetric outer barrier by about 1.5–2 MeV. Removing spurious quadrupole vibrations from the mean-field states by configuration mixing of the angular momentum projected mean-field states lowers both the ground state and the isomeric state by a few 100 keV. For ^{240}Pu, this effect is more pronounced for the isomer, which lowers its excitation energy even further, but it cannot be expected that this will be the same for all actinides.

In this section we will confine ourselves to the heights of the inner and outer barrier as well as the excitation energies of the isomeric states while postponing a thorough discussion of the potential landscapes to future work. As our goal is the extrapolation of the models to superheavy nuclei, a discussion of these key quantities suffices.

The selection of even-even nuclei for this study is $^{230}_{90}$Th$_{140}$, $^{234}_{90}$Th$_{144}$, $^{234}_{92}$U$_{142}$, $^{238}_{92}$U$_{146}$, $^{238}_{94}$Pu$_{144}$, $^{242}_{94}$Pu$_{148}$, $^{246}_{94}$Pu$_{152}$, $^{242}_{96}$Cm$_{146}$, $^{246}_{96}$Cm$_{150}$, $^{250}_{96}$Cm$_{154}$, and $^{250}_{98}$Cf$_{152}$, which is only every second known nucleus in neutron number. We omit Fm isotopes as there are two competing paths at the outer barrier, and there is no continuous axial path for the inner barrier for some Skyrme forces [36].

Figure 2 compares calculated and experimental heights of the inner barrier. In the case of the inner barrier, the comparison of data with values obtained from axial calculations is somewhat dangerous, as the static inner barrier is known to be triaxial and the energy gain through triaxial deformation may differ for each force. Still, there are several conclusions that can be safely drawn from Fig. 2. Our selection of forces suggests that there is a difference between SHF and RMF models. All Skyrme forces predict that the inner barrier increases with neutron number up to $N=150$, most pronounced for SLy6. The Z dependence of the barrier height is most pronounced for SkI3 and SkI4, the Skyrme forces with an extended spin-orbit interaction, while it is negligible for SkP, the only force in our sample with the large effective mass $m_0^*/m=1.0$, cf. Table I. One might suspect that the corresponding large level density suppresses shell effects compared to the other forces. On the other hand, for the two RMF forces the barriers stay nearly constant with N, and show an increase with Z only. This finding suggests a significant difference in shell structure between the SHF and RMF models. Experimental data do not show any significant dependence on N or Z at all, they just fall off a few 100 keV with mass number. From our present calculations, it cannot be decided if adding triaxiality will give a similar trend.

There is also a difference in absolute height between SHF and RMF. With the exception of SkP, the inner barriers from

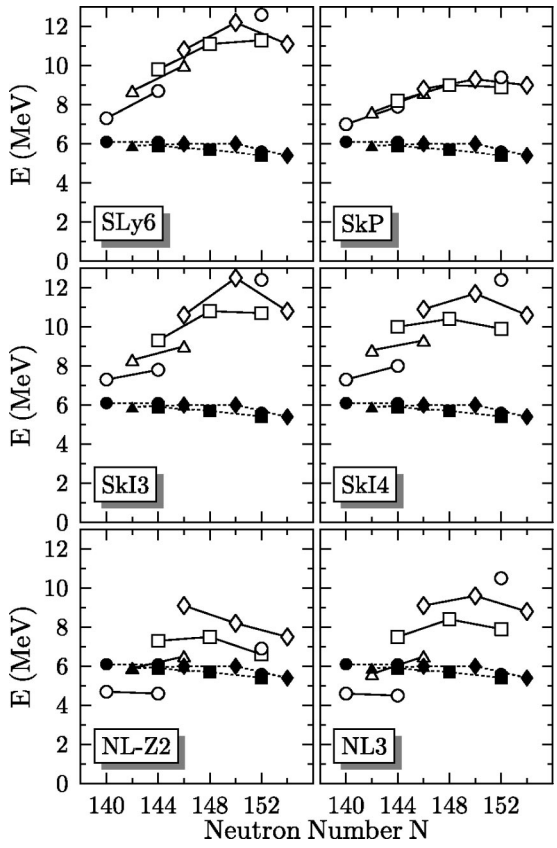

FIG. 2. Height of the inner barrier from axial and reflection-symmetric calculations. Th($Z=90$), U($Z=92$), Pu($Z=94$), Cu($Z=96$), and Cf($Z=98$) isotopes are denoted by open circles (for $N=140, 142$), open triangles, open squares, open diamonds, and again open circles ($N=152$), respectively. Experimental data (full symbols) are taken from Ref. [29]. Data points for the same element are connected by lines.

SHF are significantly higher by about 2 MeV than those obtained within the RMF. This is reflected in the values for the mean deviation of the inner barrier height $(1/n)\Sigma_{i=1}^{n}|\Delta E_i|$ from the experimental value in MeV is 4.5 (SLy6), 2.7 (SkP), 4.1 (SkI3), 4.1 (SkI4), 1.5 (NL-Z2), and 2.3 (NL3), respectively, although this quantity is of limited significance. Angular momentum projection will lower the barrier by about 1 MeV, and one can speculate only about the effect of triaxiality and other correlations on the trends with N and Z. It is tempting to assume that, when including these missing corrections, the SHF might still overestimate the barriers of the heavier nuclei but be on the right order for the lighter ones, while the RMF will underestimate the barriers of Th isotopes already on the mean-field level.

The outer barrier heights as predicted by the various mean-field forces are shown in Fig. 3. For the outer barrier, it can be expected that our calculations cover all necessary degrees of freedom, so data and calculated values can be directly compared. There are differences in absolute barrier height. With a mean deviation of the outer barrier height in MeV of 2.2 (SLy6), 4.7 (SkP), 1.4 (SkI3), 3.8 (SkI4), 1.2 (NL-Z2), and 0.8 (NL3), respectively, SkI3, NL-Z2, and in particular NL3 give a quite good description of the barrier

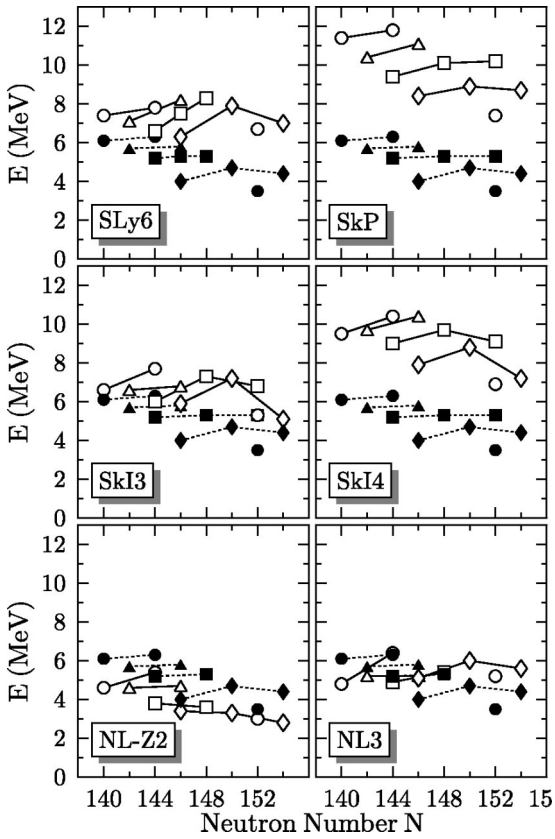

FIG. 3. The same as Fig. 2, but for the outer barrier.

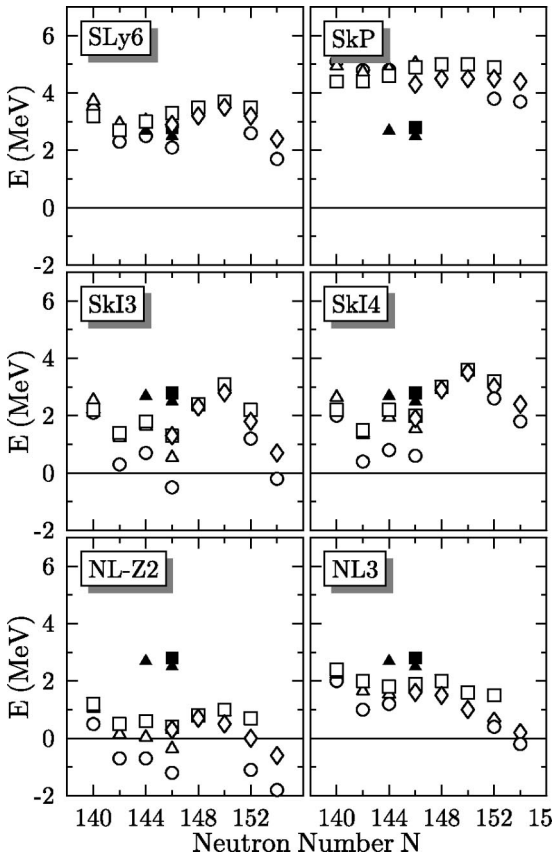

FIG. 4. Excitation energy of the isomer, obtained from axial calculations.

height on the mean-field level. The differences found for the barrier height seem to manifest themselves mainly in an overall offset, while all models and forces predict quite similar trends of the barrier heights with N and Z, a bit more pronounced for Skyrme forces, and a bit more damped for NL-Z2. The good news is that this overall trend is quite close to the experimental findings.

As barriers from NL-Z2 are already always smaller than the experimental values, there is no room left for correlation effects. For shapes around the outer barrier, the (missing) rotational correction can be expected to be about 1.5 MeV larger than for the ground state of a well-deformed nucleus. When removing those 1.5 MeV from the outer barrier heights shown in Fig. 3, the barriers from the RMF are too low, in particular for NL-Z2, where not much will be left.

The excitation energy of the fission isomer is displayed in Fig. 4. We have added also results obtained for the nuclei with neutron numbers between those used to investigate the barriers above. To the best of our knowledge, only three experimental values for superdeformed 0^+ states in even-even nuclei are available so far from spectroscopy in the superdeformed and normal-deformed wells, which are ^{236,8}U and ^{240}Pu; see the recent collection of data in Ref. [70]. There are more superdeformed levels known in some other adjacent even and odd nuclei, but their quantum numbers could not be established so far. They all have in common that their excitation energy is at least 2 MeV, which also sets some constraints to our calculations. These values are also consistent with the data obtained from fits to fission-isomer excitation functions, see, e.g., Ref. [71].

Although the sparse data do not allow for a detailed analysis, there are a few conclusions that can be drawn. On the mean-field level, SkP gives rather high energies and overestimates the data by about 2 MeV. Values from SLy6 are scattered around the data. RMF models predict very low excitation energies. The Skyrme interactions SkI3 and SkI4 with extended spin-orbit interactions also underestimate the known excitation energies at least for certain elements. It is noteworthy that SkI3, NL3, and particularly NL-Z2 predict the superdeformed state to be the ground state for some actinide nuclei, in contradiction with experimental knowledge about the spectroscopy and decay of those nuclei. It was already noticed in Ref. [40] for selected examples that the RMF underestimates the excitation energy of the fission isomer. This seems to be a general shortcoming of the RMF model, at least of most, if not all, of its standard parametrizations. This finding is not restricted to actinide nuclei, but was also observed for superdeformed states in the neutron-deficient $A \approx 190$ region [72,73], where it can be cured to some extent taking additional information about the spherical shell structure of ^{208}Pb into account during the fit of the force parameters [73]. The overbinding of the fission isomer can be expected to become even more pronounced when corrections for breaking of rotational and other symmetries are considered.

From our small selection of Skyrme forces, it is hard to disentangle the influence of the effective mass and of the various spin-orbit functionals from the influence of the actual

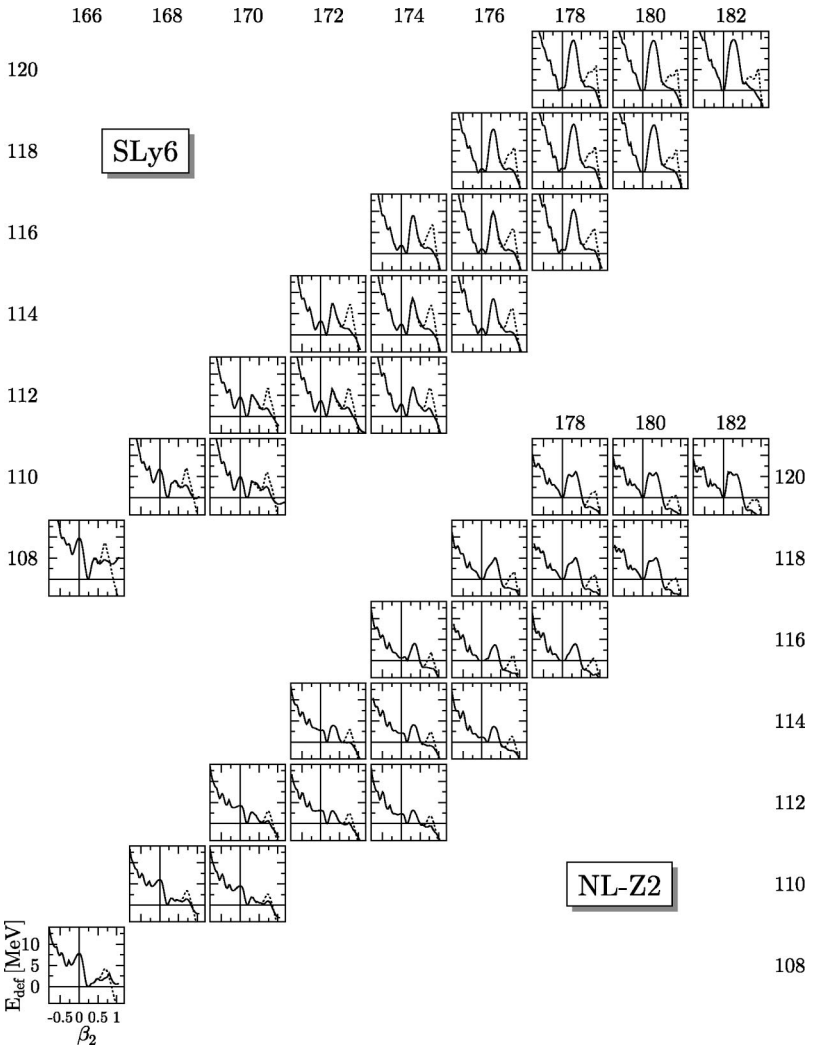

FIG. 5. Axial fission barriers for the Skyrme force SLy6 (top) and the relativistic force NL-Z2 (bottom). Solid (dashed) lines denote the reflection-asymmetric (reflection-symmetric) path.

fitting procedure on the predictions for barrier heights. It is tempting to correlate the large deformation energy obtained with SkP with its large effective mass, but this is ruled out by recent Skyrme-HFB mass fits with effective mass around 1.0 that deliver much smaller barriers [74] than SkP. Since NL-Z2 and NL3 have the same functional form, the tendency of NL3 to larger barriers must result from the different strategies to adjust the force.

It is a bit surprising that the differences in surface tension visible in Table I are not reflected in the inner barrier heights and cannot be solely responsible for the differences obtained for outer barrier heights and fission isomers. Shell effects seem to play a much larger role for these quantities than the nuclear matter properties. For the forces in our sample, the difference in surface tension seems to be compensated by other features of the forces through the fit. However, when the influence of shell effects is suppressed by comparing predictions of pairs of otherwise identically fitted forces with different surface tension, one finds indeed the expected difference, see Ref. [41] for the example of the Skyrme interactions SLy4 and SLy6 and the RMF forces NL1 and NL-Z.

Summarizing, a differences in the models, can be recognized. SHF gives usually higher barriers than RMF. In comparison with experimental data, it seems that the RMF predictions are too low for barriers and fission isomers. These findings were already hinted in earlier investigations of actinide [40,41] and superheavy nuclei [36], but emerge even more clearly for the present systematic investigation of nuclei.

In the following section we will see how these trends translate to superheavy nuclei.

V. POTENTIAL LANDSCAPES

Figure 5 provides a summary view of the deformation energy curves along the fission paths for all SHE under consideration here for the Skyrme interaction SLy6 and the relativistic mean-field force NL-Z2. The full lines denote the asymmetric fission path and the dashed lines the symmetric fission path (which coincide at small deformations). The global trends are common for both forces (and also the others employed in this study) and in qualitative agreement with earlier studies in mic-mac and semiclassical models.

(1) There is a gradual transition from well-deformed nuclei with $\beta_2 \approx 0.3$ around the deformed $Z=108$ and $N=162$ shell closures to spherical shapes approaching $N=184$. Note that earlier studies suggest that the neutron number is more

important than the proton number to determine the ground-state shape.

(2) Intermediate systems around $Z=114$, $N=174$ have two distinct prolate and oblate minima at small deformation. On the basis of our axial calculations it is not clear if this leads to shape coexistence in these nuclei as concluded on similar grounds in Refs. [75–77]. Calculations including triaxial degrees of freedom suggest that for some, or perhaps all, of these systems the prolate and oblate "minima" are connected through triaxial shapes without a barrier [78].

(3) While the ground-state deformation moves to smaller values, also the saddle point is shifted to smaller deformations. This means that the width of the fission barrier is not necessarily larger for nuclei with spherical shell closures.

(4) The transitional nuclei in between belong to a regime of low fission barriers. This is consistent with the current (still sparse) experimental knowledge. The recent data from Dubna interpreted as the α-decay chain of $^{292}116$ indicate that fission is the preferred decay channel for $^{280}110_{170}$, but not for the heavier nuclides in this chain [8].

(5) Above $Z=108$, the static fission path switches from symmetric to asymmetric fission.

(6) For most of the nuclei above $Z \geqslant 110$ considered here, reflection-asymmetric shape degrees of freedom remove completely the outer barrier that is well known from actinide nuclei, leading to a single-humped fission barrier only.

(7) The superdeformed minima around $\beta_2 \approx 0.5$ obtained from reflection-symmetric calculations with NL-Z2 for $^{298}118_{176}$ in Ref. [76] and $^{292}116_{176}$, $^{288}114_{174}$, $^{284}112_{172}$, and $^{280}110_{172}$ in Ref. [77] are not stable with respect to octupole distortions, which makes the conclusions about superdeformed ground states of superheavy nuclei drawn in Refs. [76,77] questionable. This finding is not completely general as for some forces there remains a very small asymmetric barrier.

The general features of these trends are easily understood in the more intuitive language of the mic-mac models (although they apply, of course, to the self-consistent models as well). For nuclei at the lower end of the region investigated here, the potential energy surface from the LDM is rather flat around the spherical point and drops off fast at prolate deformations about $\beta_2 \approx 0.7$, cf. Fig. 7 in Ref. [35]. The structures seen in Fig. 5 are mainly determined by the variation of the shell correction with deformation. The maximum of the shell correction follows the shell closures from the deformed $Z=108$ and $N=162$ to the spherical $N=184$ shell. The potential wells are deepest in the vicinity of closed shells. With increasing Z, the plateau is shifted toward oblate deformations, while the LDM surface drops at smaller and smaller prolate deformations, which cannot be counterweighted by the variation of E_{shell}. With that the saddle point moves in toward smaller deformations. For larger systems than those discussed here the potential energy surface becomes also unstable on the oblate side.

Figure 5 gives also an idea where triaxiality might play a significant role. Whenever the deformation energy is smaller on the oblate side than for the same deformation on the prolate side outside the prolate saddle point, oblate shapes might be unstable through a triaxial path. Of course this is neither a sufficient nor necessary condition.

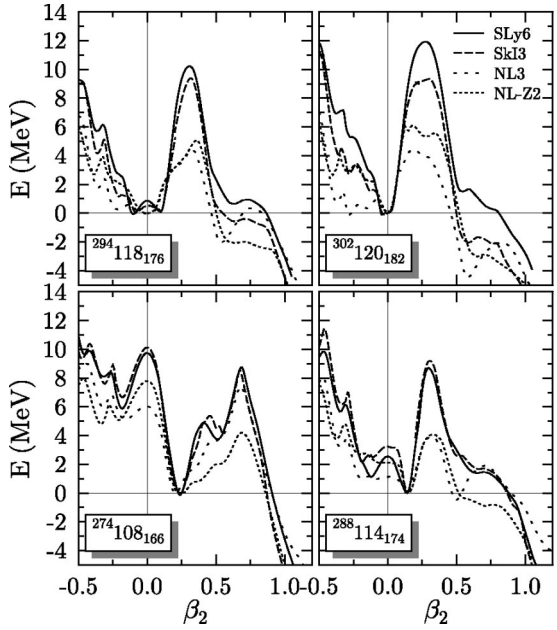

FIG. 6. The fission barriers of four selected nuclei normalized to the ground-state for four mean-field parametrizations as indicated. Shown is always the energetically favored fission barrier.

While there is overall qualitative agreement among the two forces (and models), there are significant differences at a quantitative level. The RMF force NL-Z2 predicts lower barriers when going toward heavy systems than the Skyrme interaction SLy6. This is confirmed when directly comparing the deformation energy for selected nuclei, see Fig. 6. $^{274}_{166}Hs_{108}$ is a well-deformed nucleus located at the edge of the "rock of stability" around $^{270}_{162}Hs_{108}$, $^{302}_{182}120$ is close to the spherical neutron shell $N=184$, while the other two are located in the transitional region. The figure compares more forces, now two from SHF (SLy6 and SkI3) and two from RMF (NL3 and NL-Z2).

There are two kinds of differences. First, the systematic difference between SHF and RMF models which we saw already for the actinides, with the RMF giving smaller barriers, persists to superheavy systems, and second, an additional difference between the two RMF parametrizations NL-Z2 and NL3 concerning the outer barrier occurs, with NL3 being the only force predicting a double-humped barrier for the heavier systems.

Comparing the potential energy curves from NL-Z2 and SLy6 at small deformation for the heaviest nuclei, one sees also some differences concerning how strongly the nuclei are driven to sphericity. Comparing nuclides in the "northeastern" corner of Fig. 5, the onset of spherical ground states is predicted to be earlier with NL-Z2 than with SLy6. This reflects the different predictions for shell closures from both models [42,43]. While NL-Z2 (like all other standard RMF forces) predicts strong $Z=120$ and $N=172$ shells and a weak $N=184$ shell, SLy6 gives a strong $N=184$ shell and a weak $Z=120$ shell, which is not sufficient to guarantee a spherical ground state of this nucleus for nonmagic neutron number. Therefore nuclei at the upper end of Fig. 5 are much more driven to sphericity when calculated with NL-Z2 than with SLy6.

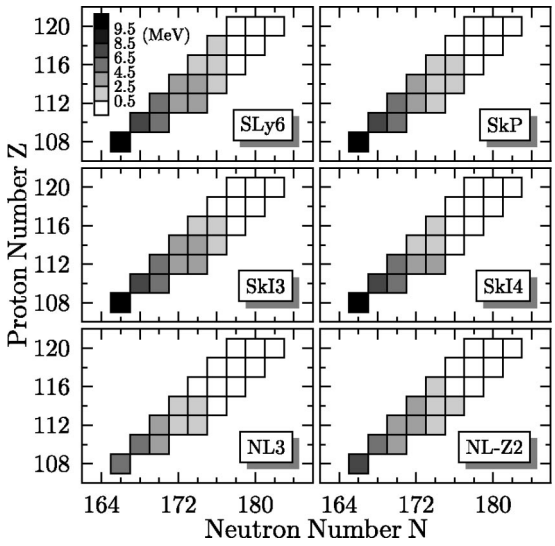

FIG. 7. Deformation energy for the lowest minimum at small deformation ($\beta_2 \leqslant 0.4$) for the nuclides and forces as indicated. White squares denote deformation energies smaller than 0.5 MeV. See the main text for a detailed description.

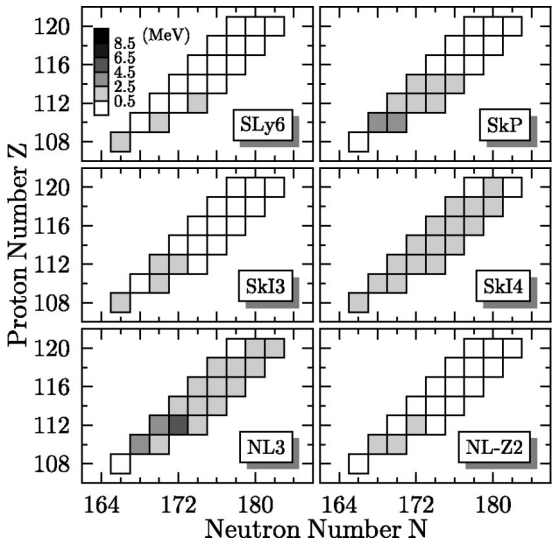

FIG. 8. Height of the outer, usually asymmetric, fission barrier with respect to the isomeric state. White squares indicate a second bump smaller than 0.5 MeV.

VI. CHARACTERISTIC QUANTITIES

The basic features of all the deformation energy surfaces shown in the previous plots can be characterized by a few key numbers, i.e., the ground-state deformation energy and the height of the inner fission barrier and the outer barrier, which will be discussed in this section.

A. Ground-state deformation energy

The ground-state deformation energy, i.e., the energy difference between the spherical shape and the (possibly deformed) ground state, is plotted in Fig. 7. We consider only small deformations $\beta_2 \leqslant 0.4$. Zero deformation energy always indicates a spherical ground state, as we do not find coexisting well-deformed minima at the same energy as the spherical configuration.

We see that all models and parametrizations predict a transition from deformed nuclei around $Z=108$, $N=162$ to spherical $N=184$ in agreement with earlier studies [35,79]. These deformation energies correspond to strongly prolate deformations at the lower corner of our selection of nuclei. For higher Z values, a shape isomerism is established with two minima on the prolate and oblate side having approximately the same energy and only small deformations of $\beta_2 \approx \pm 0.15$. Thus far the general trends agree. There are differences in quantitative detail, most prominently the fact that RMF predicts systematically lower deformation energies than SHF.

It is to be noted that in SHE the neutron number most often determines the ground-state shape, while a magic proton number might not prevent deformation. This seems to be a general feature of all self-consistent models [35,79], and can also be observed in mic-mac models, which predict deformed $Z=114$ isotopes [80,81] far off $N=184$. This is due partially to the overall larger shell correction energy of the spherical neutron shells compared to the proton shells [82], and partially to the existence of many deformed proton shell closures in the region $108 \leqslant Z \leqslant 120$, which drive nuclei with nonmagic neutron number toward deformation.

B. Existence of shape isomers

The existence of a shape (or fission) isomer with deformation around $\beta \approx 1.0$ is a prominent feature of actinide nuclei [59]. A fission isomer necessarily requires an outer fission barrier. The height of the outer barrier with respect to the isomeric state is shown in Fig. 8. All forces and models confirm the earlier finding that the outer barrier fades away for transactinide nuclei, see e.g. Ref. [36]. An exception is NL3, which predicts a substantial outer barrier for most nuclei, cf. also Fig. 6. As NL-Z2 usually does not show a fission isomer, this cannot be a general feature of the RMF model, but has to be a particularity of the NL3 parametrization. Similarly, SkI4 is an exception among the Skyrme interactions. Most nuclear matter properties of NL3 and NL-Z2 are very close, the same holds for the Skyrme interactions SkI4, SkI3, and SLy6. This suggests that the height of the outer barrier is mainly determined by shell structure, not the average liquid-drop properties. Remember that SkI4 employs a nonstandard spin-orbit interaction which leads to single-particle spectra different from those of the other self-consistent models at spherical shape [43].

C. Saddle-point height

A most interesting feature of SHE is the stability against spontaneous fission. The fission half-life can be computed from a tunneling dynamics in the shape degrees of freedom [83]. Input to that are the collective masses along the fission path and the fission barriers. We aim here at a mere comparison of stability between the different forces. To that end, we assume that the collective masses are almost similar in all

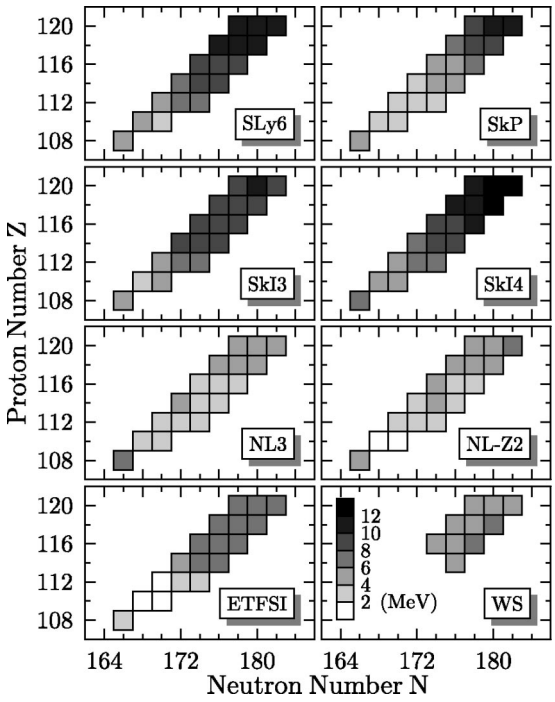

FIG. 9. The height of the symmetric inner barrier calculated in axial symmetry for the models and forces as indicated. We have also added ETFSI taken from Ref. [30] and mic-mac results obtained within the YPE+WS model from Ref. [26].

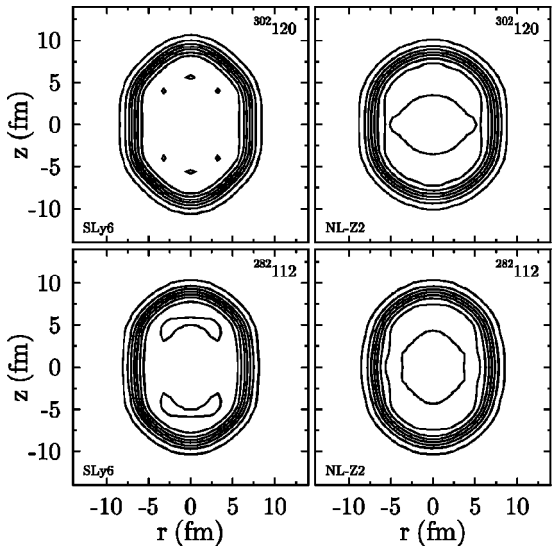

FIG. 10. Contour plots of the mass density distribution for the saddle-point configurations of the nuclei $^{282}112_{170}$ (lower panels) and $^{302}120$ (upper panels) as predicted by the forces SLy6 (left) and NL-Z2 (right). The z axis is the symmetry axis. The contour lines correspond to the densities 0.01, 0.03, …, 0.15 and 0.17 fm^{-3}.

cases and confine the discussion to the height of the (inner) axial fission barrier as key quantity. Keep in mind that the numbers given for the barrier height represent an upper limit due to possible lowering through triaxial shapes.

The systematics of the fission barriers for all nuclei and mean-field forces considered here are shown in Fig. 9. We have added results from two other large-scale calculations, one employing the semi-classical ETFSI approach [30] and the other within the mic-mac approach [26]. In both cases axial shapes which allow for reflection asymmetry are assumed, similar as in our calculations. The mic-mac fission barriers from Ref. [26] are dynamical barriers, i.e. the barrier which lies on the fission path that minimizes the multidimensional action.

All models and forces agree that there is a regime of low fission barriers around $Z=110$, but the (axial) barriers increase again when going toward $N=184$. There are, however, significant differences among the models. Comparing the fully self-consistent models, the barriers from RMF are much lower than those from SHF.

And even among the various SHF forces, we see differences in the barriers. It is again SkI4 with its particular spin-orbit force which shows the largest barriers. Here it is noteworthy that SkI4 predicts largest stability for $Z=120$ although it places the magic shell closure at $Z=114$ [43]. This shows once again that "magicity" is something different from stability as was argued also in Ref. [82].

The ETFSI calculations give barriers that have almost the same size as the ones from the RMF forces, with the difference that they produce a bit smaller barriers at the lower end and larger regions with more stable nuclei. Similarly, the barriers from the mic-mac rather correspond to the estimates from the RMF forces. The self-consistent SHF results deliver the highest barriers throughout.

For two nuclei and the forces SLy6 and NL-Z2, the saddle-point shapes are shown in Fig. 10. In all cases, compact nuclear shapes are obtained. The saddle-point deformation decreases slightly from values around $\beta_2=0.32$ obtained with both forces for ^{274}Hs, to $\beta_2=0.28$ obtained with SLy6 and $\beta_2=0.18$ predicted by NL-Z2, respectively, for $^{302}120$. Note that for NL-Z2 there exists no pronounced saddle point, since the barrier is rather flat (see Fig. 6).

Figure 9 also shows fission barriers calculated within the mic-mac method [26]. The trends are remarkably different from the self-consistent models. A maximum of stability is found around $Z=116$ and less stability for larger systems. Effective mass $m^*/m=1$ cannot be the reason because SkP with $m^*/m=1$ behaves as all other SHF and RMF. We can only speculate about possible explanations. There might be differences in the smooth part of the self-consistent models, e.g., in higher-order terms missing in the mic-mac models or even the curvature term (all of which do not necessarily have the right structure in self-consistent models); or the effect comes from the different shell structure between the Folded-Yukawa potential used in the mic-mac calculations and self-consistent models [43] (although the difference among, e.g., SkI4 and NL-Z2 is quite significant, while the global trend of the barriers is not).

It can be speculated that this is a consequence of missing shape degrees of freedom, either in missing higher-order deformations in the mic-mac method or in the radial density distribution. It is well known that multipole moments at least up to $\ell=8$ have to be taken into account to obtain the full shell effect around $^{270}_{108}\mathrm{Hs}_{162}$ [84]. It can be expected that even more shape degrees of freedom are necessary to get the full shell effect for the even more complex saddle-point configu-

TABLE II. Comparison of fission barriers (see text). Experimental data are taken from Ref. [13]. The assignment of the neutron number has some uncertainty, therefore the same experimental barrier appears for two nuclei in the list.

Nucleus	Expt.	NL3	NL-Z2	SLy6	SkI3	SkI4	SkP
$^{284}112_{172}$	5.5	3.38	2.99	6.06	6.75	6.03	2.77
$^{286}112_{174}$	5.5	3.41	3.16	6.91	7.52	6.97	2.77
$^{288}114_{174}$	6.7	3.87	4.08	8.12	8.75	8.11	4.02
$^{290}114_{176}$	6.7	3.56	3.70	8.52	8.15	8.67	4.31
$^{292}116_{176}$	6.4	3.81	3.74	9.35	8.77	9.62	5.67
$^{294}116_{178}$	6.4	3.80	3.96	9.59	8.61	10.93	6.50

ration. The standard mic-mac models also assume that protons and neutrons have the same deformation. An exploration of the consequences of this constraint in the framework of the self-consistent Gogny force is given in Ref. [85]. Imposing the same deformation for neutrons and protons leads to larger barriers of the order of 1 MeV in actinides. A similar effect can be expected for SHE. Even more severe might be the parametrization of the radial density distribution in mic-mac models. There is no radial degree of freedom at all, although it is well known that changing the surface diffuseness might significantly change the ground-state shell correction of SHE. The current parametrizations of mic-mac models also prevent "semibubble" density distributions that might appear at the upper end of the nuclei in Fig. 9.

Although each missing degree of freedom causes a loss in binding energy, the deformation dependence of the various effects can be expected to be very different. Depending on if the missing energy is larger at the ground state or around the saddle point the fission barriers are either increased or decreased. This might explain the difference in the global trend between mic-mac and self-consistent models.

Table II compares our calculated barrier heights with the lower limits of the barriers of some very heavy nuclei recently deduced from an analysis of the available data for fusion and fission [13]. Surprisingly, these experimentally estimated barrier heights are similar, or even slightly larger, than that of actinide nuclei in the ^{240}Pu region. Experimental and calculated values are in agreement for the Skyrme forces SLy6, SkI3, and SkI4, while both RMF forces and the Skyrme interaction SkP significantly underestimate the barrier.

Although the barrier heights are comparable, the lifetimes corresponding to these barriers are much shorter than for actinide nuclei as the barriers are much narrower. For the adjacent $^{280}_{170}110$, a fission lifetime of about $T_{1/2}=7.6^{+5.8}_{-2.3}$ s was reported in Ref. [8]. This is quite short but two orders of magnitude longer than results of the mic-mac model, which predict about 10^{-1} s [26]. As those heavy nuclei are solely stabilized by shell effects [86], reliable predictions will be a difficult task for any model.

VII. SEARCH FOR UNDERLYING MECHANISMS

The above results on the fission barriers and its trends toward the heaviest SHE show systematic differences between SHF and RMF. In this section, we want to ponder a bit about possible reasons. For the further discussion it is useful to distinguish between the macroscopic part of the models (which determines the nuclear matter properties and the average trends), and the microscopic part (which determines the actual shell structure). As we will see, it is not yet fully clear which part is responsible for the observed systematic differences.

A. Macroscopic aspects

It is well known that most nuclear matter properties from SHF and RMF models differ significantly, see e.g. Ref. [37] and references therein. In lowest order, the barrier heights can be expected to scale with the surface energy coefficient $a_{\rm surf}$. With the exception of NL3, however, the values for $a_{\rm surf}$ are quite close for all forces used here, see Table I. NL3 gives in most cases smaller (inner) barriers in spite of its larger surface energy coefficient.

If the differences seen in Fig. 6 are rooted in the macroscopic part, another bulk property than $a_{\rm surf}$ has to be responsible. It is unlikely that this is the volume energy because it is basically independent of the nuclear shape. The situation is more involved for the volume symmetry energy, coefficient $a_{\rm sym}$. At first glance, the volume energy also scales with the nuclear volume, but there is an implicit surface effect due to a correlation between the neutron skin and $a_{\rm sym}$; the skin increases with increasing $a_{\rm sym}$. A systematic study performed in Ref. [87] suggests that this relation is unique. A variation of other isovector properties as the sum rule enhancement factor $\kappa_{\rm TRK}$ or the surface-asymmetry coefficient $\kappa_{\rm sym}$ leaves the skin unchanged.

And indeed, when we calculate fission barriers with the systematically varied Skyrme forces from Ref. [87], we find that the barriers increase with decreasing $a_{\rm sym}$, while they do not change when the isovector effective mass is varied. This is consistent with our findings for the barriers, where the Skyrme forces which all have $a_{\rm sym}\approx 32$ MeV have larger barriers than the RMF forces with $a_{\rm sym}\approx 39$ MeV, cf. Table I. This correlation is not unique and might apply only to forces fitted according to the protocol of Ref. [88]. The Skyrme mass fit MSk7 [89], which follows a very different fitting strategy, has a significantly smaller $a_{\rm sym}=27.95$ MeV than the Skyrme forces used here, but predicts also significantly smaller fission barriers for heavy and superheavy nuclei [74], which are in fact similar to our RMF results. With that, a satisfying explanation of the difference between RMF and SHF concerning fission barrier heights based on macroscopic properties of the models is still missing.

B. Microscopic aspects

For nuclei with flat or unstable macroscopic potential energy surfaces the height of the fission barrier is determined by the variation of the shell correction energy $E_{\rm shell}$ with deformation. $E_{\rm shell}$ reflects the deviation of the actual density of single-particle levels around the Fermi energy $\epsilon_{\rm F}$ from an averaged level density. Pivotal for the barrier is not the absolute value of $E_{\rm shell}$, but its variation, which reflects the change of the single-particle spectra with deformation.

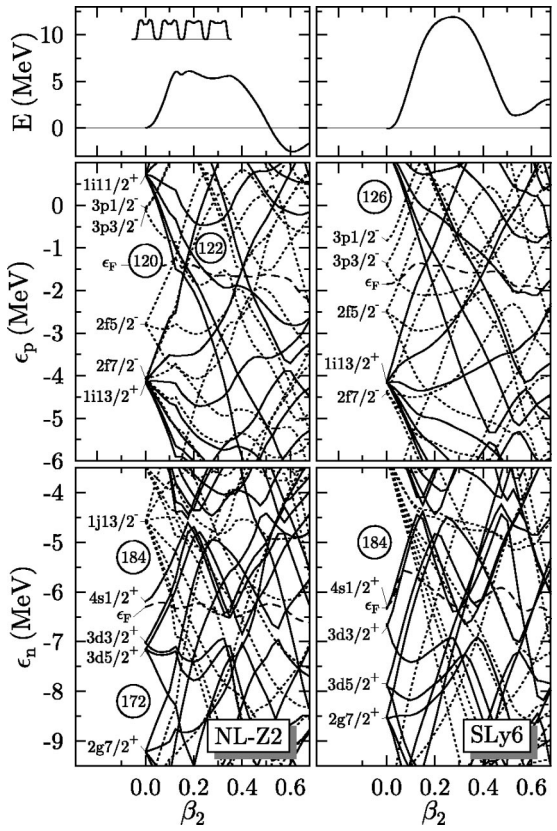

FIG. 11. Inner axial fission barrier (top), proton levels (middle), and neutron levels (bottom) for the nucleus $^{302}120$ with NL-Z2 (left) and SLy6 (right). Solid (dotted) lines in the Nilsson plots denote single-particle states with positive (negative) parity, while the dashed line plots the Fermi energy. In the upper panel for NL-Z2, the radial distribution of the total density along the *z* axis is also shown.

Nilsson plots of the single-particle energies of the nucleus $^{302}120_{182}$ as calculated with the RMF force NL-Z2 and the Skyrme interaction SLy6 are shown in Fig. 11. There are significant differences between the forces which can be traced back to their different shell structure at spherical shape ($\beta_2=0$) [42,43]. The small spin-orbit splitting of the $3p$ and $2f$ states obtained with NL-Z2 leads to a major shell closure at $Z=120$, while $Z=120$ is a subshell closure only for SLy6, which (for this neutron number) has more prominent gaps in the single-particle spectrum at $Z=114$ and $Z=126$. On the other hand, there is a huge gap in the neutron spectrum at $N=184$ for SLy6, while there are several small gaps at $N=172$, 182, and 184 for NL-Z2.

It has to be stressed, however, that for self-consistent models such Nilsson plots cannot be extrapolated very far from the N and Z they are calculated for. For deformed shapes, the self-consistent optimization of higher multipole moments when changing N and Z might change the single-particle spectra significantly. Additionally, the radial shape of the density distribution might change with nucleon numbers [34,43,90] or deformation. Figure 11 provides an example for the latter. At small deformation NL-Z2 predicts a semi-bubble shape for $^{302}120_{182}$ (see the small inserts in the upper panel), which around $\beta_2\approx0.12$ changes abruptly into a more

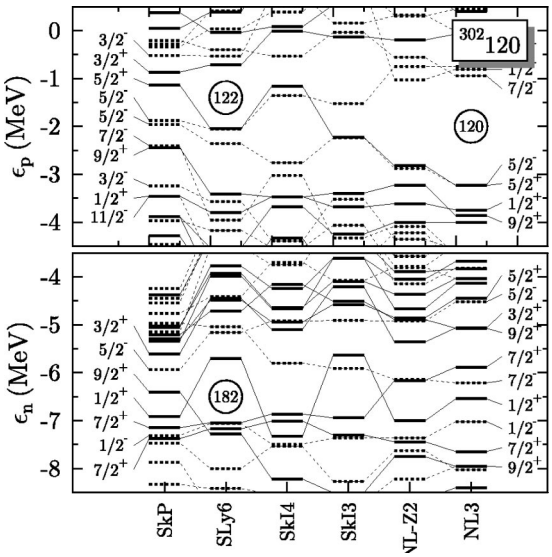

FIG. 12. Single-particle spectra in the superdeformed configuration obtained from reflection-symmetric calculations for $^{302}120_{182}$.

regular density distribution, thereby causing the discontinuity in the single-particle spectra at that deformation. The semi-bubble shape reduces the spin-orbit splitting (cf. the proton $2f$, $3p$, or neutron $3d$ states). The appearance of such semi-bubble shapes is force dependent, for SLy6 it occurs for $Z=120$ only at smaller neutron numbers around $N=172$. For a more detailed discussion of this phenomenon see Refs. [34,43,90].

Comparing the spectra from NL-Z2 and SLy6 at spherical shape, there is another significant difference besides the spin-orbit splitting. The highly degenerated $1i_{11/2^+}$ proton and $1j_{13/2^-}$ neutron states above the Fermi energy are much lower for NL-Z2 than for SLy6. This does not yet lead to a significantly smaller (total) shell correction for NL-Z2 ($E_{\rm shell}=-13.1$ MeV) than for SLy6 ($E_{\rm shell}=-14.1$ MeV) [82], but their splitting with deformation brings more of these levels close to the Fermi energy around the fission barrier for NL-Z2, which might be the reason for the difference between NL-Z2 and SLy6. From looking at the single-particle spectra in Fig. 11 alone, however, this cannot be decided. To resolve this issue, a calculation of the shell correction for deformed shapes along the strategy of Ref. [82] seems highly desirable.

The single-particle spectra at the spherical point also determine the existence or nonexistence of the reflection-asymmetric outer barrier, and with that of the fission isomer. At deformations around $\beta_2\approx0.5$, there are several single-particle states originating from the intruder and the major shells above and below coming close to the Fermi energy, see Fig. 12 for the example of $^{302}120_{182}$. Spectra for other nuclei in this region look quite similar. Octupole deformation mixes states with the same angular momentum but opposite parity, so depending on the actual level ordering it will increase or decrease the level density at the Fermi surface. The differences in the relative distance of the single-particle states found at spherical shape [43] are reflected in the spectra for these very deformed shapes. For example, the subtle shift in single-particle energies between the RMF forces

NL-Z2 and NL3 removes the outer asymmetric barrier for the former, but not the latter. The single-particle spectra at spherical shape including those far above and below the Fermi energy have to be described with very high precision to decide if there exist superdeformed states in superheavy elements.

VIII. CONCLUSIONS

We have investigated the systematics of fission barriers in superheavy elements with $Z=108, \ldots, 120$ as predicted by self-consistent mean-field models. As typical representatives, we employed the nonrelativistic Skyrme-Hartree-Fock (SHF) model as well as the relativistic mean-field (RMF) model, and for each case, we used a selection of different parametrizations to explore the variances in the predictions. All calculations have been done with axial symmetry but allowing for reflection-asymmetric shapes.

As a benchmark for our mean-field models and forces, a selection of actinide nuclei ranging from Th to Cf isotopes has been utilized to study the predictions for the inner and outer axial barriers as well as the excitation energies of the isomer. Overall, a model dependence of the results has surfaced. RMF forces tend to lower, and often too low, barriers and excitation energies, while most Skyrme forces tend to higher values, which sometimes leads to an overestimation on the mean-field level.

For superheavy nuclei all models and forces agree on the systematic trends concerning the fission barriers, ground-state deformations, and fission modes. There are differences in detail. Fission isomers are generally suppressed in superheavy elements, with the exception of the RMF force NL3 in our sample. For larger nuclei, there emerge large and systematic discrepancies between SHF and RMF concerning the barrier heights, reaching a factor of 2 for $Z=120$. This amplifies and confirms the tendency which has been demonstrated for actinides. The factor of 2 in fission barriers around $Z=120$ means in absolute numbers that SHF fission barriers are about 5 MeV larger and this amounts to many orders of magnitude longer fission lifetimes. Moreover, the SHF forces employed here predict also barriers larger than the more phenomenological mic-mac models. The reason for the systematic difference between SHF and RMF have yet to be found out. We suspect that the difference is caused by a different shell structure in the models. This point deserves more investigation.

The further systematic trends are shared by SHF and RMF. There is a transition from well-deformed ground states around $Z=108$ to nearly spherical ones at $Z=120$, which develops through very soft nuclei which might exhibit shape isomerism. Also there is a marked breakdown of fission stability around $Z=110$ in agreement with experimental findings where the α chains of superheavy elements are limited at the lower end by fission.

The axially symmetric fission barriers are, of course, only a first indicator of fission stability (to be more precise, an upper limit). One needs yet to include triaxial degrees of freedom and to model the dynamics of fission to obtain lifetimes. Taking into account the results from actinides and superheavy nuclei, the mean-field models used in this study seem to deliver lower (and probably too low—RMF) and upper (SHF) limits for the barrier heights. It is yet difficult to map these differences on special and isolated features of the models, which remains an urgent and important task for the near future.

ACKNOWLEDGMENTS

We thank W. Greiner, Yu. Ts. Oganessian, M. Samyn, and V. I. Zagrebaev for inspiring discussions which initiated this work, as well as S. Schramm for help with coding problems. This work was supported in part by Bundesministerium für Bildung und Forschung (BMBF), Grant No. 06 ER 808, and by the PAI-P5-07 of the Belgian Office for Scientific Policy. M.B. acknowledges financial support by the European Community.

[1] S. Hofmann, Rep. Prog. Phys. **61**, 639 (1998).
[2] S. Hofmann and G. Münzenberg, Rev. Mod. Phys. **72**, 733 (2000).
[3] P. Armbruster, Annu. Rev. Nucl. Part. Sci. **50**, 411 (2000).
[4] Ch. E. Düllmann *et al.*, Nature (London) **418**, 859 (2002).
[5] S. Hofmann *et al.*, Eur. Phys. J. A **10**, 5 (2001).
[6] Yu. Ts. Oganessian *et al.*, Eur. Phys. J. A **5**, 68 (1999).
[7] Yu. Ts. Oganessian *et al.*, Phys. Rev. Lett. **83**, 3154 (1999); Nature (London) **400**, 209 (1999); Phys. Rev. C **62**, 041604(R) (2000).
[8] Yu. Ts. Oganessian *et al.*, Phys. Rev. C **63**, 011301(R) (2001); Eur. Phys. J. A **15**, 201 (2002).
[9] S. Hofmann *et al.*, Eur. Phys. J. A **14**, 147 (2002).
[10] J. R. Nix, Phys. Lett. **30B**, 1 (1969).
[11] J. Grumann, U. Mosel, B. Fink, and W. Greiner, Z. Phys. **228**, 371 (1969).
[12] P. Reiter *et al.*, Phys. Rev. Lett. **82**, 509 (1999); M. Leino *et al.*, Eur. Phys. J. A **6**, 63 (1999); P. Reiter *et al.*, Phys. Rev. Lett. **84**, 3542 (2000); R.-D. Herzberg *et al.*, Phys. Rev. C **65**, 014303 (2002).
[13] M. G. Itkis, Yu. Ts. Oganessian, and V. I. Zagrebaev, Phys. Rev. C **65**, 044602 (2002).
[14] D. L. Hill and J. A. Wheeler, Phys. Rev. **89**, 1102 (1953).
[15] C. R. Chinn, J.-F. Berger, D. Gogny, and M. S. Weiss, Phys. Rev. C **45**, 1700 (1992); S. J. Krieger, P. Bonche, H. Flocard, P.-H. Heenen, and M. S. Weiss, Nucl. Phys. **A572**, 384 (1994); S. J. Krieger, P. Bonche, H. Flocard, P.-H. Heenen, R. Mehrem, and M. S. Weiss, Phys. Rev. C **54**, 2399 (1996).
[16] N. Rowley, G. R. Satchler, and P. H. Stelson, Phys. Lett. B **254**, 25 (1991); N. Rowley, Nucl. Phys. **A538**, 205c (1992); Y. Abe, Y. Aritomo, T. Wada, and M. Ohta, J. Phys. G **23**, 1275 (1997); G. G. Adamian, N. V. Antonenko, W. Scheid, and V. V. Volkov, Nucl. Phys. **A633**, 409 (1998); R. Smolańczuk, Phys. Rev. C **63**, 044607 (2001); V. Yu. Denisov and S. Hof-

mann, *ibid.* **61**, 034606 (2000); V. Yu. Denisov and W. Nörenberg, Eur. Phys. J. A **15**, 375 (2002); V. I. Zagrebaev, Phys. Rev. C **64**, 034606 (2001); V. I. Zagrebaev, Y. Aritomo, M. G. Itkis, Yu. Ts. Oganessian, and M. Ohta, *ibid.* **65**, 014607 (2002).

[17] W. D. Myers and W. J. Swiatecki, Nucl. Phys. **81**, 1 (1966).

[18] V. M. Strutinsky, Nucl. Phys. **A95**, 420 (1967); **A122**, 1 (1968).

[19] M. Bolsterli, E. O. Fiset, J. R. Nix, and J. L. Norton, Phys. Rev. C **5**, 1050 (1971); M. Brack, J. Damgård, A. S. Jensen, H. C. Pauli, V. M. Strutinsky, and C. Y. Wong, Rev. Mod. Phys. **44**, 320 (1972); J. R. Nix, Annu. Rev. Nucl. Part. Sci. **22**, 66 (1972); P. Möller and J. R. Nix, Nucl. Phys. **A229**, 269 (1974).

[20] P. Möller and S. G. Nilsson, Phys. Lett. **31B**, 283 (1970); C. Gustafson, P. Möller, and S. G. Nilsson, *ibid.* **34B**, 349 (1971); P. Möller, Nucl. Phys. **A192**, 529 (1972).

[21] V. V. Pashkevich, Nucl. Phys. **A133**, 400 (1969); S. E. Larsson, I. Ragnarsson, and S. G. Nilsson, Phys. Lett. **38B**, 269 (1972); U. Götz, H. C. Pauli, and K. Junker, *ibid.* **39B**, 436 (1972).

[22] E. O. Fiset, and J. R. Nix, Nucl. Phys. **A193**, 647 (1972); J. Randrup, C. F. Tsang, P. Möller, S. G. Nilsson, and S. E. Larsson, *ibid.* **A217**, 221 (1973); J. Randrup, S. E. Larsson, P. Möller, S. G. Nilsson, K. Pomorski, and A. Sobiczewski, Phys. Rev. C **13**, 229 (1976).

[23] H. C. Pauli, T. Ledergerber, and M. Brack, Phys. Lett. **34B**, 264 (1971); H. C. Pauli and T. Ledergerber, Nucl. Phys. **A173**, 398 (1971).

[24] P. Möller, J. R. Nix, and W. J. Swiatecki, Nucl. Phys. **A469**, 1 (1987); **A492**, 349 (1989); **A549**, 84 (1992); P. Möller and A. Iwamoto, Phys. Rev. C **61**, 047602 (2001).

[25] A. Baran, K. Pomorski, A. Łukasiak, and A. Sobiczewski, Nucl. Phys. **A361**, 83 (1981); A. Sobiczewski, Z. Patyk, and S. Ćwiok, Phys. Lett. B **186**, 6 (1987); Z. Patyk, J. Skalski, A. Sobiczewski, and S. Ćwiok, Nucl. Phys. **A502**, 591 (1989); Z. Patyk and A. Sobiczewski, *ibid.* **A533**, 132 (1991); R. Smolańczuk, J. Skalski, and A. Sobiczewski, Phys. Rev. C **52**, 1871 (1995).

[26] R. Smolańczuk, Phys. Rev. C **56**, 812 (1997).

[27] R. A. Gherghescu, J. Skalski, Z. Patyk, and A. Sobiczewski, Nucl. Phys. **A651**, 237 (1999).

[28] W. D. Myers and W. J. Swiatecki, Phys. Rev. C **60**, 014606 (1999); Nucl. Phys. **A601**, 141 (1996).

[29] A. Mamdouh, J. M. Pearson, M. Rayet, and F. Tondeur, Nucl. Phys. **A644**, 389 (1998); **A648**, 282(E) (1999).

[30] A. Mamdouh, J. M. Pearson, M. Rayet, and F. Tondeur, Nucl. Phys. **A679**, 337 (2001).

[31] A. K. Dutta, J. M. Pearson, and F. Tondeur, Phys. Rev. C **61**, 054303 (2000).

[32] R. W. Hasse and W. D. Myers, *Geometrical Relationships of Macroscopic Nuclear Physics* (Springer, Berlin, 1988).

[33] J.-F. Berger, L. Bitaud, J. Dechargé, M. Girod, and S. Peru-Dessenfants, in *Proceedings of the 34th Internatinal Workshop on Gross Properties of Nuclei and Nuclear Exitations, Hirschegg, Austria*, 1996, edited by H. Feldmeier, J. Knoll, and E. Nörenberg (GSI, Darmstadt, 1996), p. 43; J.-F. Berger, L. Bitaud, J. Dechargé, M. Girod, and K. Dietrich, Nucl. Phys. **A685**, 1c (2001).

[34] J. Dechargé, J.-F. Berger, M. Girod, and K. Dietrich, Nucl. Phys. **A716**, 55 (2003).

[35] S. Ćwiok, J. Dobaczewski, P.-H. Heenen, P. Magierski, and W. Nazarewicz, Nucl. Phys. **A611**, 211 (1996).

[36] M. Bender, K. Rutz, P.-G. Reinhard, J. A. Maruhn, and W. Greiner, Phys. Rev. C **58**, 2126 (1998).

[37] M. Bender, P.-H. Heenen, and P.-G. Reinhard, Rev. Mod. Phys. **75**, 121 (2003).

[38] A. K. Dutta and M. Kohno, Nucl. Phys. **A349**, 455 (1980).

[39] M. Brack, C. Guet, and H.-B. Håkansson, Phys. Rep. **123**, 275 (1985).

[40] K. Rutz, J. A. Maruhn, P.-G. Reinhard, and W. Greiner, Nucl. Phys. **A590**, 680 (1995).

[41] M. Bender, K. Rutz, P.-G. Reinhard, and J. A. Maruhn, Eur. Phys. J. A **7**, 467 (2000).

[42] K. Rutz, M. Bender, T. Bürvenich, T. Schilling, P.-G. Reinhard, J. A. Maruhn, and W. Greiner, Phys. Rev. C **56**, 238 (1997).

[43] M. Bender, K. Rutz, P.-G. Reinhard, J. A. Maruhn, and W. Greiner, Phys. Rev. C **60**, 034304 (1999).

[44] J. Dobaczewski, H. Flocard, and J. Treiner, Nucl. Phys. **A422**, 103 (1984).

[45] E. Chabanat, P. Bonche, P. Haensel, J. Meyer, and R. Schaeffer, Nucl. Phys. **A635**, 231 (1998); **A643**, 441(E) (1998).

[46] P.-G. Reinhard and H. Flocard, Nucl. Phys. **A584**, 467 (1995).

[47] G. A. Lalazissis, J. König, and P. Ring, Phys. Rev. C **55**, 540 (1997).

[48] M. Farine, J. Coté, J. M. Pearson, and W. Stocker, Z. Phys. A **309**, 151 (1982).

[49] D. Von Eiff, W. Stocker, and M. K. Weigel, Phys. Rev. C **50**, 1436 (1994).

[50] W. Stocker (private communication).

[51] M. Samyn and J. M. Pearson (private communication).

[52] M. Warda, J. L. Egido, L. M. Robledo, and K. Pomorski, Phys. Rev. C **66**, 014310 (2002).

[53] M. Bender, K. Rutz, P.-G. Reinhard, and J. A. Maruhn, Eur. Phys. J. A **8**, 59 (2000).

[54] M. Bender, Doctoral Dissertation, J. W. Goethe-Universität Frankfurt am Main, 1998.

[55] V. Blum, G. Lauritsch, J. A. Maruhn, and P.-G. Reinhard, J. Comput. Phys. **100**, 364 (1992).

[56] K. Rutz, Doctoral Dissertation, J. W. Goethe-Universität Frankfurt am Main, 1998.

[57] P.-G. Reinhard, Nucl. Phys. **A306**, 19 (1978); P.-G. Reinhard and K. Goeke, Rep. Prog. Phys. **50**, 1 (1987).

[58] H. Flocard, P. Quentin, A. K. Kerman, and D. Vautherin, Nucl. Phys. **A203**, 433 (1973).

[59] S. M. Polikanov *et al.*, Sov. Phys. JETP **15**, 1016 (1962); H. J. Specht, J. Weber, E. Konecny, and D. Heunemann, Phys. Lett. **41B**, 43 (1972); H. J. Specht, Rev. Mod. Phys. **46**, 773 (1974); R. Vandenbosch, Annu. Rev. Nucl. Part. Sci. **27**, 1 (1977); S. Bjørnholm and J. E. Lynn, Rev. Mod. Phys. **52**, 725 (1980); V. Metag, D. Habs, and H. J. Specht, Phys. Rep. **65**, 1 (1980); P. G. Thirolf and D. Habs, Prog. Part. Nucl. Phys. **49**, 325 (2002).

[60] C. E. Bemis, Jr., F. K. McGowan, J. L. C. Ford, Jr., W. T. Milner, P. H. Stelson, and R. L. Robinson, Phys. Rev. C **8**, 1466 (1973).

[61] M. Hunyadi *et al.*, Phys. Lett. B **505**, 27 (2001).

[62] H. X. Zhang, T. R. Yeh, and H. Lancman, Phys. Rev. C **34**, 1397 (1986); J. Blons, Nucl. Phys. **A502**, 121c (1989).

[63] H. Flocard, P. Quentin, D. Vautherin, M. Véneroni, and A. K. Kerman, Nucl. Phys. **A231**, 176 (1974).
[64] M. Girod and B. Grammaticos, Phys. Rev. C **27**, 2317 (1983); J.-F. Berger, M. Girod, and D. Gogny, Nucl. Phys. **A428**, 23c (1984); **A502**, 85c (1989).
[65] V. Blum, J. A. Maruhn, P.-G. Reinhard, and W. Greiner, Phys. Lett. B **323**, 262 (1994).
[66] J. Bartel, P. Quentin, M. Brack, C. Guet, and H.-B. Håkansson, Nucl. Phys. **A386**, 79 (1982).
[67] P.-H. Heenen, J. Dobaczewski, W. Nazarewicz, P. Bonche, and T. L. Khoo, Phys. Rev. C **57**, 1719 (1998).
[68] S. Takahara, N. Tajima, and N. Onishi, Nucl. Phys. **A642**, 461 (1998).
[69] M. Bender and P.-H. Heenen (unpublished).
[70] B. Singh, R. Zywina, and R. B. Firestone, Nucl. Data Sheets **97**, 241 (2002).
[71] H. C. Britt, S. C. Burnett, B. H. Erkkila, J. E. Lynn, and W. E. Stein, Phys. Rev. C **4**, 1444 (1971); H. C. Britt, M. Bolsterli, J. R. Nix, and J. L. Norton, *ibid.* **7**, 801 (1973).
[72] K. Heyde, C. De Coster, P. Van Duppen, M. Huyse, J. L. Wood, and W. Nazarewicz, Phys. Rev. C **53**, 1035 (1996).
[73] T. Niksic, D. Vretenar, P. Ring, and G. A. Lalazissis. Phys. Rev. C **65**, 054320 (2002).
[74] M. Samyn and S. Goriely (unpublished).
[75] S. K. Patra, Cheng-Li Wu, C. R. Praharaj, and Raj K. Gupta, Nucl. Phys. **A651**, 117 (1999).
[76] Zhongzhou Ren and H. Toki, Nucl. Phys. **A689**, 691 (2001).
[77] Zhongzhou Ren, Phys. Rev. C **65**, 051304(R) (2002).
[78] S. Ćwiok, P.-H. Heenen, and W. Nazarewicz (unpublished).
[79] T. Bürvenich, K. Rutz, M. Bender, P.-G. Reinhard, J. A. Maruhn, and W. Greiner, Eur. Phys. J. A **3**, 139 (1998).
[80] P. Möller and J. R. Nix, J. Phys. G **20**, 1681 (1994).
[81] P. Möller, J. R. Nix, and K.-L. Kratz, At. Data Nucl. Data Tables **66**, 131 (1997).
[82] A. T. Kruppa, M. Bender, W. Nazarewicz, P.-G. Reinhard, T. Vertse, and S. Ćwiok, Phys. Rev. C **61**, 034313 (2000); M. Bender, W. Nazarewicz, and P.-G. Reinhard, Phys. Lett. B **515**, 42 (2001).
[83] S. G. Nilsson and I. Ragnarsson, *Shapes and Shells in Nuclear Structure* (Cambridge University Press, Cambridge, 1995).
[84] Z. Patyk and A. Sobiczewski, Phys. Lett. B **256**, 307 (1991); **A533**, 132 (1991).
[85] J.-F. Berger and K. Pomorski, Phys. Rev. Lett. **85**, 30 (2000).
[86] Z. Patyk, A. Sobiczewski, P. Armbruster, and K.-H. Schmidt, Nucl. Phys. **A491**, 267 (1989).
[87] P.-G. Reinhard, Nucl. Phys. **A649**, 305c (1999).
[88] J. Friedrich and P.-G. Reinhard, Phys. Rev. C **33**, 335 (1986).
[89] S. Goriely, F. Tondeur, and J. M. Pearson, At. Data Nucl. Data Tables **77**, 311 (2001); F. Tondeur, S. Goriely, J. M. Pearson, and M. Onsi, Phys. Rev. C **62**, 024308 (2000).
[90] J. Dechargé, J.-F. Berger, K. Dietrich, and M. S. Weiss, Phys. Lett. B **451**, 275 (1999).